Edge effects on the electromagnetic response of inhomogeneous type-II superconductors

O. A. Hernández-Flores, C. E. Ávila-Crisóstomo, P. L. Valdés-Negrin, and C. Romero-Salazar

Escuela de Sistemas Biológicos e Innovación Tecnológica, Universidad Autónoma Benito Juárez de Oaxaca, Av. Universidad s/n 68120 Oaxaca de Juárez, Oaxaca, México.

R. Cortés-Maldonado

Tecnológico Nacional de México, IT de Apizaco, Av. Instituto Tecnológico s/n, Apizaco, 90300, Tlaxcala, México.

F. Pérez-Rodríguez

Instituto de Física, Benemérita Universidad Autónoma de Puebla, Edificio IF-1, Ciudad Universitaria, Puebla, Pue. 72570, México.

Received 22 July 2022; accepted 20 February 2023

From a macroscopic point of view, the edges of a type II superconductor are degraded non-homogeneous regions compared with the bulk of the sample. This paper presents numerical simulations of a long superconducting bar with square cross section subjected to an axial external magnetic field, the edges effect on its electromagnetic properties is studied. The edges of the sample are modeled as finite width regions with lower critical current density than the rest of the material. The simulations are based on a continuum electrodynamics model which describes the magnetic induction dynamics of partially penetrated states. Unlike a simpler homogeneous superconductor, in an inhomogeneous material rough flux fronts are formed. It was established that the stochastic profile of the current density produces jets of magnetic flux near a macrodefect.

Keywords: Rough magnetic flux fronts; type II superconducting material; continuum electrodynamics model.

DOI: https://doi.org/10.31349/RevMexFis.69.040502

1. Introduction

Macroscopic inhomogeneities influence strongly the superconducting properties, they can promote a glass transition of the disorder flux-line lattice [1, 2] or produce a negative differential conductivity [3]. In non-homogeneous regions occurs an exchange of flow between adjacent pinning regions, draining the lower pinning region [4], they stimulate a nonlinear response to microwave radiation [5, 6]. Moreover, intricate and spectacular magnetic manifestations are hidden at the transient regime due to its short duration [7–9], as the external magnetic field becomes stable, the system approaches the stationary regime (critical state). Furthermore, various technologies that use superconducting materials work in the non-stationary regime, where the inhomogeneities have a notable influence on vortex dynamics. Defects are inevitable in the manufacture of monolithic superconducting materials, they modify their superconducting properties and represent a problem for its potential technological applications [10–13]. In particular, the edges of a superconducting sample are considered as regions with magnetic properties different from the bulk. In this study, an inhomogeneous superconducting material is modeled assuming lower current-carrying capacity at the edges than in the rest of the material, in other words, the material has an inhomogeneous critical current density j_c [14–16]. The superconducting material is under a time-varying external field, due to the lower quality of the edges, the incursion of the field into the material is promoted and a rough flux front is created. It is desirable to understand the changes of the electromagnetic properties of the superconducting sample as the flux front is propagated.

The paper is organized as follows: Section 2 presents the equations that describe the magnetodynamics in the continuum electrodynamics framework; the model for the inhomogeneities is described in Sec. 3; the numerical methodology is explained in Sec. 4; the results for the time-depedent distributions of the magnetic induction and current density are presented in Sec. 5; in Sec. 6 the main conclusions are pointed out.

2. Macroscopic electrodynamic approach

We consider a type-II superconducting bar of square cross section $a \times a$ and length $l \gg a$, aligned with the $z-$axis. The bar is subjected to an homogeneous and time varying external magnetic field $\mathbf{H}_a = H_a\hat{\mathbf{z}}$, with magnitude $H_a = R_R t$ and ramp rate R_R. In this configuration $\mathbf{H} \parallel \mathbf{B} \parallel \hat{\mathbf{z}}$, the electromagnetic fields depend on x and y, and $\mathbf{j} = j_x\hat{\mathbf{x}} + j_y\hat{\mathbf{y}}$. The lower critical field is considered $H_{c1} \ll H_a$, thus the linear relation $B_z = \mu_0 H_z$ is valid. The magnetic flux entering or leaving the superconducting material is mediated by the geometric barriers, Bean-Levingston barriers and Meissner currents, its influence is appreciable when the external field is

close to H_{c1}. Even when they were not taken into account in this work, one way to incorporate their effects is employing a nonlinear $B(H)$ relation [17]. In the macroscopic approach, the magnetodynamics is described by the Ampere and Faraday laws, both laws can be written in the single equation:

$$\frac{\partial B_z}{\partial t} = \frac{1}{\mu_0}\left\{\frac{\partial}{\partial x}\left(\rho\frac{\partial B_z}{\partial x}\right)+\frac{\partial}{\partial y}\left(\rho\frac{\partial B_z}{\partial y}\right)\right\}, \qquad (1)$$

here, it is used a material law $\mathbf{E} = \rho\mathbf{j}$ with a resistivity $\rho = \rho(B, j)$. Equation (1) is a partial differential equation subjected to the initial (IC) and boundary (BC) conditions,

$$\begin{aligned} \text{IC:} & B_z(x, y, t=0) = f(x, y), \\ \text{BC:} & B_z(x=0, y, t) = B_z(x=a, y, t) = \mu_0 H_a, \\ & B_z(x, y=0, t) = B_z(x, y=a, t) = \mu_0 H_a. \end{aligned} \qquad (2)$$

We model the resistivity through the equation

$$\rho = \xi\rho_n \frac{j_{c0}}{j_c}\frac{(j/j_c)^m}{1+(j/j_c)^m}, \qquad (3)$$

where ρ_n is the resistivity at $T = T_c$, j_{c0} is the maximum critical current supported by the material, j_c is the critical current density and ξ a dimensionless parameter. This function includes both the flux creep regime and the thermally-assisted flux-flow (TAFF). Indeed, in the flux creep regime, observed at small values of the current density j ($j \ll j_c$), the resistivity ρ increases with j as the power law:

$$\rho = \xi\rho_n \frac{j_{c0}}{j_c}\left(\frac{j}{j_c}\right)^m, \qquad (4)$$

where m is the creep exponent. On the other hand, at large values of j ($j \gg j_c$), *i.e.* in the TAFF regime, the resistivity

$$\rho \approx \xi\rho_n \left(\frac{j_{c0}}{j_c}\right), \qquad (5)$$

and the relation between the electric field $\mathbf{E}$ and the current density $\mathbf{j}$ has the Omh's law form [18–20]. Furthermore, function (3) is also valid for the critical state if the critical electric field is defined as $E_c = \xi\rho_n j_{c0}/2$. To close the set of equations a critical current model is required, we chose the Kim-Anderson model:

$$j_c = \frac{j_{c0}}{1+\dfrac{B}{B^*}}, \qquad (6)$$

where B^* is a parameter.

3. Model for the inhomogeneous borders

The inhomogeneous borders are defined as a virtual square hollow bar of length $l \gg a$ and wall thickness Δa embedded in the bar. The borders have superconducting properties different from the bulk (see the sketch at the inset of panel (a) of Fig. 1).

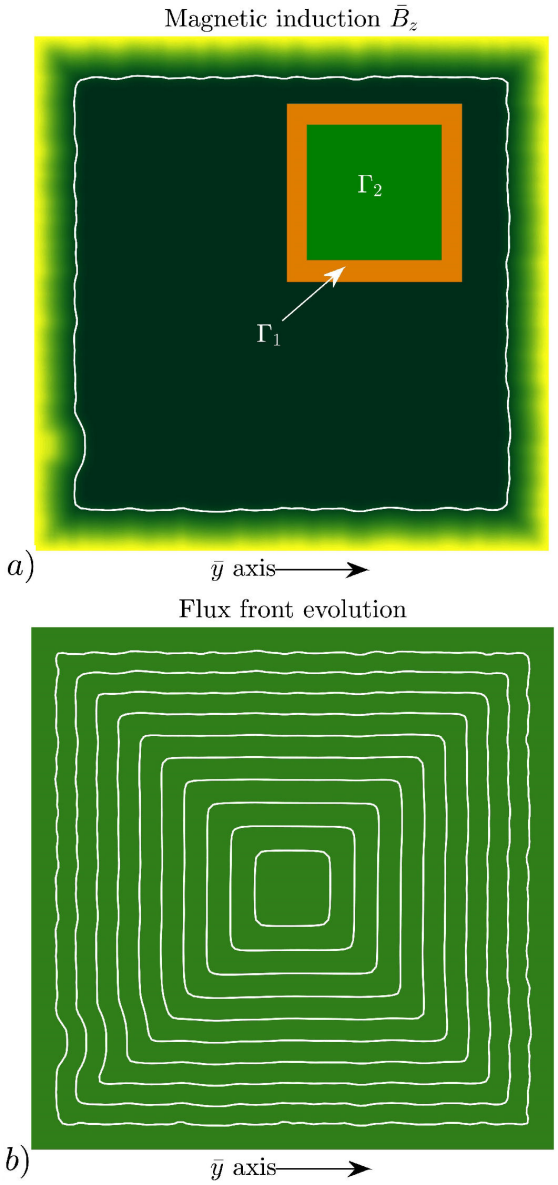

FIGURE 1. a) Pseudocolor plot of the magnetic induction, the inhomogeneous edges created a rough flux front (white line). Inset. Sketch of the zones Γ_1 and Γ_2. b) Evolution of the flux front (white lines) for $\bar{B}_a \leq \bar{B}_{\max}$. A "macrodefect" located at the left edge of both figures had been included. From the colormap, the yellow intensity indicates a higher field value, while the green intensity indicates a lower field value.

Because of the magnetic field is axial, the electromagnetic quantities are independent of z and the problem is two-dimensional ($2D$), with every $z-$plane equivalent to each other. We denote the bar cross section as $\Gamma = \Gamma_1 \cup \Gamma_2$, where Γ_1 is the edge region and Γ_2 is the bulk region. It is assumed a completely homogeneous Γ_2 region, with maximum critical current density $j_{c0}(\Gamma_2) = j_0$, however, this is not completely true in real superconducting monoliths. For the purposes of this study, homogeneity in the bulk is required since we are interested on the flux front propagation.

We consider a constant magnetic permeability $\mu = \mu_r\mu_0 = \mu_0$ and a variable resisitivity in Γ. Every change on the current-carrying properties of the inhomogeneous superconductor is through the critical current density $j_c = j_{c0}(\Gamma)/(1 + B/B^*)$. In our study, $j_{c0}(\Gamma_1) < j_{c0}(\Gamma_2)$ is chosen, that is, the area Γ_1 is a degraded area. This is reasonable since superconducting samples are susceptible to physical changes, either by handling in the laboratory, continuous interaction with an external magnetic field or due the manufacturing process.

We introduce a mathematical model of the inhomogeneous zone whose equation is:

$$j_{c0}(\Gamma_1) = (1-\Delta) j_0 \xi(\Gamma_1) \cos(8\pi y) \cos(8\pi x) + \Delta,$$

where $\xi(\Gamma_1)$ is a random number uniformly distributed between zero and one, the parameter $0 < \Delta \leq 1$ is a measure of the degradation of the superconducting properties at the edges.

4. For the numerical performance

To solve the set of Eqs. (1)–(6) numerically, it is convenient to write them in a dimensionless form. Four basic quantities are chosen and written in terms of characteristic quantities:

$$x = a\bar{x}, \qquad y = a\bar{y}, \qquad t = t_0\bar{t}, \qquad B_z = B_0\bar{B}_z.$$

where the characteristic magnetic induction $B_0 = \mu_0 a j_0$ is constructed from $j_0 = j_{c0}(\Gamma_2)$, which is the maximum current that the superconducting material supports without dissipation; t_0 is a characteristic time. We write the resistivity as $\rho = \rho_n\bar{\rho}$ where ρ_n is the normal state resistivity. The dimensionless dynamical equation is written as follows:

$$\frac{\partial \bar{B}_z}{\partial \bar{t}} = \frac{t_0}{t_1}\left\{\frac{\partial}{\partial \bar{x}}\left(\bar{\rho}\frac{\partial \bar{B}_z}{\partial \bar{x}}\right) + \frac{\partial}{\partial \bar{y}}\left(\bar{\rho}\frac{\partial \bar{B}_z}{\partial \bar{y}}\right)\right\}, \tag{7}$$

where $t_1 = \mu_0 d^2/\rho_n$. The respective dimensionless initial and boundary conditions are:

$$\begin{aligned} \text{IC:} & \bar{B}_z(\bar{x}, \bar{y}, \bar{t}=0) = f(\bar{x}, \bar{y}), \\ \text{BC:} & \bar{B}_z(\bar{x}=0, \bar{y}, \bar{t}) = \bar{B}_z(\bar{x}=1, \bar{y}, \bar{t}) = \bar{B}_a, \\ & \bar{B}_z(\bar{x}, \bar{y}=0, \bar{t}) = \bar{B}_z(\bar{x}, \bar{y}=1, \bar{t}) = \bar{B}_a. \end{aligned} \tag{8}$$

here $\bar{B}_a = \bar{H}_a = \bar{R}_R\bar{t}$ and $\bar{R}_R = R_R t_0/B_0$. Finally, the resistivity is written as

$$\bar{\rho} = \xi \frac{\bar{j}_{c0}}{\bar{j}_c} \frac{\left(\frac{\bar{j}}{\bar{j}_c}\right)^m}{1 + \left(\frac{\bar{j}}{\bar{j}_c}\right)^m}, \tag{9}$$

where $\bar{j}_{c0} = j_{c0}/j_0$ and $\bar{j} = j/j_0$.

To solve the system of Eqs. (7)–(9) numerically we use the method of lines (MOL, [21]), next, we explain briefly in what such a methodology consists. Consider a mesh of $N \times M$ nodes denoted by (x_i, y_j). Each node will have a time-varying magnetic induction $B_z^{ij} = B_z(x_i, y_j, t)$. Faraday's law of induction can be written as:

$$\frac{\partial B_z}{\partial t} = \{\nabla \times \mathbf{E}\}_z.$$

Using the defined mesh, we denote the spatial discretization of $\{\nabla \times \mathbf{E}\}_z$ as $F^{ij}(t)$. As we can see, it is built a system of NM ordinary differential equations with the form:

$$\frac{dB_z^{ij}}{dt} = F^{ij}(t), \tag{10}$$

subjected to the initial condition $B_z^{ij}(t_{ini}) = f(t_{ini})$ (in our case $f(t_{ini} = 0) = 0$). The boundary conditions must be incorporated into the ODE system, this is done by substituting $\partial B_z^{kl}/\partial_t = \partial B_a/\partial_t$ into (10), where (x_k, y_l) are the nodes located at the boundaries.

5. Results

Numerical simulations were performed to obtain the magnetic induction and current density distributions in the superconducting bar. To present the electromagnetic quantities we used a pseudocolor plot. According to the colormap, the yellow intensity indicates the larger values, the green intensity indicates intermediate values and the darker the lower values. All color maps are normalized since in this work we are not interested in the magnitude of the electromagnetic quantities, but how they are spatially distributed in the superconducting sample.

The numerical simulations were performed in Matlab R2015a on a mobile workstation with Intel(R) Core(TM) i5-2520M CPU @ 2.50 GHz, 8 GB RAM, Windows 10 (64 bit). A mesh of 100×100 nodes (x_i, y_j) was used, $B_0 = 1\text{T}$, $a = 2.65 \times 10^{-3}\text{m}$, $\rho_n = 10^{-6}\ \Omega\cdot\text{m}$, $t_1 = 10^{-5}\text{s}$, $j_{c0}(\Gamma_2) = j_0 = 2.5 \times 10^8 \text{A/m}^2$, $B^* = 1\text{T}$ and $t_0 = 1\text{s}$. The external magnetic field $\mu_0 H_a = R_R t$ varied linearly with time at a ramp rate of $R_R = 0.01\text{T/s}$. The numerical experiment was performed as follows:

1. The inhomogeneous edges were generated by $j_{c0}(\Gamma_1)$. A "macrodefect" was included at the left edge of the sample.
2. The applied field was increased linearly with a ramp rate $\bar{R}_R = 0.01$ until the maximum value $\bar{B}_{\max} = 0.3$ was reached.
3. Starting from $\bar{B}_{\max}$, the intensity of the applied field was decreased linearly down to zero.

According to the mesh size, we chose the nodes contained in the region Γ_1, they were the set $(x_{1,2}, y_j)$, $(x_{99,100}, y_j)$, $(x_i, y_{1,2})$ and $(x_i, y_{99,100})$, with $i, j = 1, 2, \ldots, 99, 100$.

A square "macrodefect" was built selecting the nodes (x_m, y_n) where $m = 1, 2, 3, 4$ and $n = 21, 22, 23, 24$, in this site the maximum current density was $\bar{j}_{c0} = 0.25$.

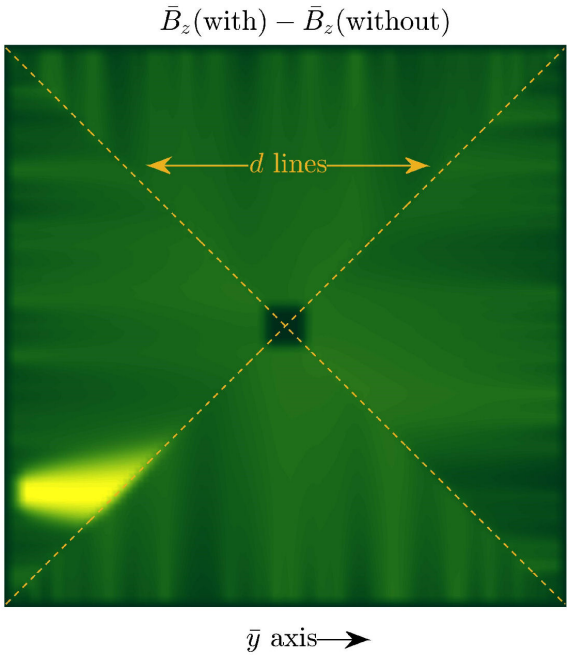

FIGURE 2. $\bar{B}_z(\text{with}) - \bar{B}_z(\text{without})$, here $\bar{B}_z(\text{with})$ is the magnetic induction in a sample with inhomogeneous edges and $\bar{B}_z(\text{without})$ is the magnetic induction of a complete homogeneous sample.

The four inhomogeneous edges were constructed with $\Delta = 0.25$ and

$$
\begin{aligned}
\bar{j}_{c0}(x_2, y_j) &= 0.75\xi_j^1 \cos(8\pi y_j) + 0.25, \\
\bar{j}_{c0}(x_1, y_j) &= j_{c0}(x_2, y_j)/2, \\
\bar{j}_{c0}(x_{99}, y_j) &= 0.75\xi_j^2 \cos(8\pi y_j) + 0.25, \\
\bar{j}_{c0}(x_{100}, y_j) &= j_{c0}(x_{99}, y_j)/2, \\
\bar{j}_{c0}(x_i, y_2) &= 0.75\xi_i^1 \cos(8\pi x_i) + 0.25, \\
\bar{j}_{c0}(x_i, y_1) &= j_{c0}(x_i, y_2)/2, \\
\bar{j}_{c0}(x_i, y_{99}) &= 0.75\xi_i^2 \cos(8\pi x_i) + 0.25, \\
\bar{j}_{c0}(x_i, y_{100}) &= j_{c0}(x_i, y_{99})/2,
\end{aligned}
$$

where $\xi_i^1, \xi_i^2, \xi_j^1, \xi_j^2$ are random numbers uniformly distributed between zero and one. The inhomogeneous edges cover around 8% of the cross section.

The system (10) is solved using the MATLAB ode113 solver. The average computation time for this numerical experiment was 40 min, while for a homogeneous superconductor the simulation time was 2 min. Such discrepancy in the simulation times is a consequence of the stringent error tolerance imposed, since high accuracy is required to find the magnetic induction at the edges.

We show at the panel (a) of Fig. 1 a pseudocolor plot of the magnetic induction in an early stage of the simulation, at this point the external field had slightly penetrated. We can

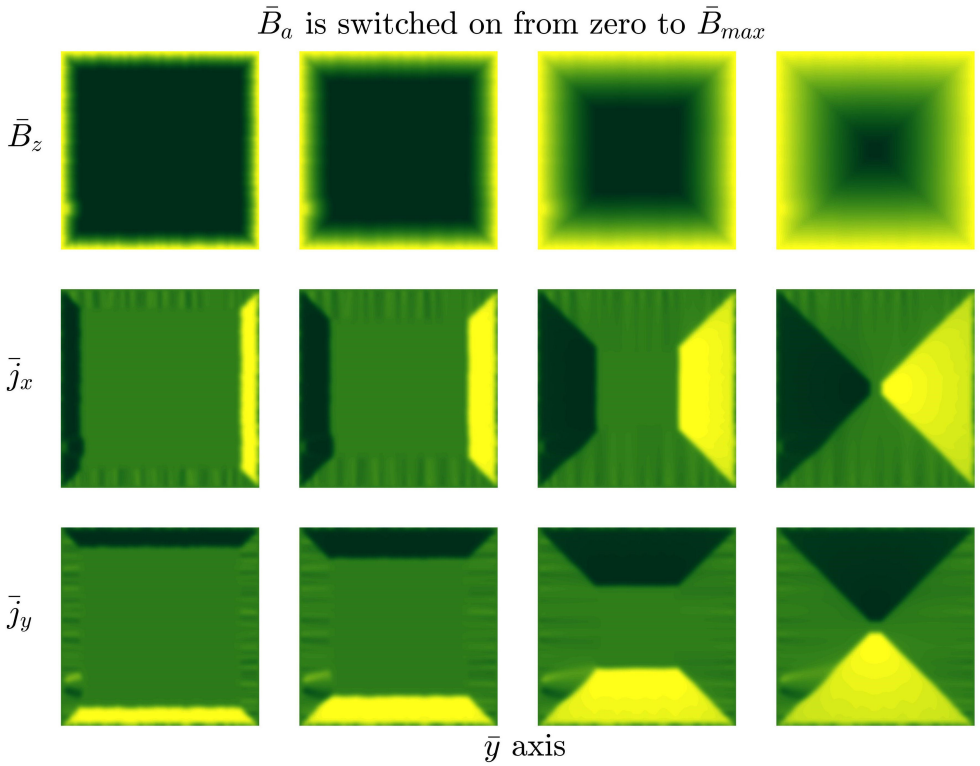

FIGURE 3. Pseudocolor plot of the magnetic induction B_z and j_x, j_y components of the current density. The external field was switched on from zero to $B_{\max}$. The yellow intensity indicates the highest field values while the green one the lowest values.

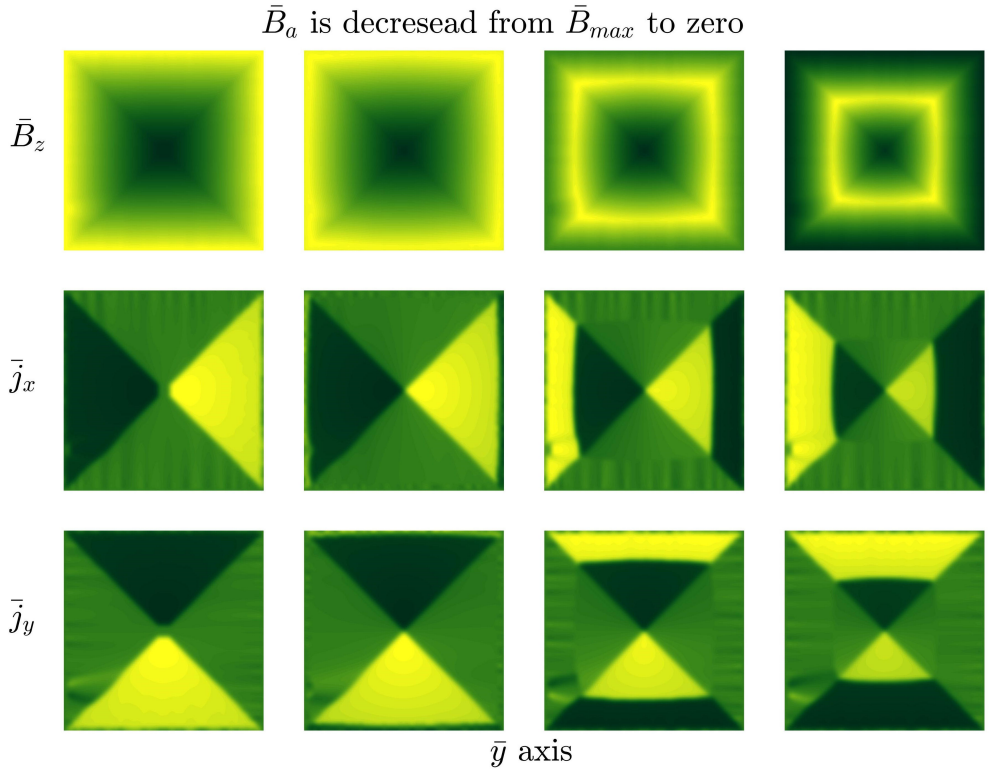

FIGURE 4. Pseudocolor plot of the magnetic induction B_z and j_x, j_y components of the current density. The external field was decreased from $B_{\max}$ to zero. The yellow intensity indicates the highest field values while the green one the lowest values.

see that the degradation of the material caused the field to penetrate irregularly, and consequently, a rough flux front was formed (we marked it with a white line). Indeed, the rough flux front was formed in the region Γ_1 and remains present even in the homogeneous zone Γ_2. Due to the non uniform flux front, gradients inevitably arised at the direction normal to the edges, and as a consequence a current density in that direction was presented. Now, panel (b) shows a set of white lines that corresponds to the rough flux front evolution for $\bar{B}_a \leq \bar{B}_{\max}$, in the region where the traveling flux front is homogeneous, the roughness was apparently lost as the field penetrated the superconducting sample. The macrodefect had been placed to show that the deflections of the current density, due to inhomogeneous edges, were less pronounced.

Figure 2 compares the distribution of the magnetic induction $\bar{B}_z(\text{with})$ of a sample with inhomogeneous edges ($\Gamma = \Gamma_1 \cup \Gamma_2$) with the magnetic induction distribution $\bar{B}_z(\text{without})$ of a complete homogeneous sample ($\Gamma = \Gamma_2$), both for the applied field $\bar{B}_a = \bar{B}_{\max}$. It is evident how the inhomogeneous edges and the "macrodefect" influenced the magnetic induction distribution in the homogeneous zone. It can be seen how the areas with the greatest degradation of the edges produced field jets, in contrast to the quadratic distribution generated by the "macrodefect". The field jets did not cross the d-lines marked with yellow dashed lines.

Figures 3 and 4 show the evolution of the magnetic induction $\bar{B}_z$ as well as the components $\bar{j}_x$ and $\bar{j}_y$ of the current density, as the external field varied with time. In Fig. 3, $\bar{B}_a$ was switched on from zero to $\bar{B}_{\max}$, as can be seen, the inhomogeneous edges affected the distributions of the magnetic induction and the current density, in early stages its influence was relevant, however they were attenuated as the external field increased. The current density components present dark and bright intercalated zones that indicates a change of direction of the supercurrent lines, these changes tend to disappear as the external field saturates the superconducting material. This behavior also occurred at the "macrodefect" although in a lesser extent. In the Fig. 4 $\bar{B}_a$ was decreased from $\bar{B}_{\max}$ to zero. The magnetic induction in $\bar{B}_{\max}$ had not penetrated completely the superconductor, this can be seen in the first column of the figure, however, in the rest of the columns the field had completely penetrated, this effect is associated with the flux creep. As in the previous figure, in the current density distribution there are dark and bright areas interspersed but inverted, that is, bright and dark areas, this is due to the change of polarity of the field. The process of change of direction of the supercurrent lines was gradual, there was a transition applied field where the supercurrent lines did not undergo changes in their direction, as illustrated the second column of graphs. Of course, in the "macrodefect" the supercurrent lines continued deflecting. In the case of the remanent field, the reversal of the superconducting currents was partial, due to a squared "mountain range" formed in the magnetic induction that limits the effect of the inhomogeneous edges. This "mountain range" was formed because the maximum applied field is practically the penetration field.

6. Concluding remarks

A computational simulation has been successfully carried out to describe, in a more realistic way and from a macroscopic point of view, a bulk superconducting material with degradation of the superconducting properties at the edges of the sample. Even when there is a clear discrepancy on the simulation time of a homogeneous sample and one with degraded edges, the simulation time was short, considering the stringent error tolerance, a modest computing capacity and the interpreted language.

We were able to confirm that the Γ_1 zone (degraded borders) induced a rough flux front (Fig. 1) in the homogeneous Γ_2 zone. The roughness, due to the stochastic profile $j_{c0}(\Gamma_1)$, produced jets of magnetic flux and the rate of magnetic flux entering took different values in Γ_1, the highest value corresponded to the greatest degraded zone. As expected, the flux front became uniform as the external field was increased, however, the distribution of magnetic induction maintained traces of roughness (Figs. 1 and 2).

The pseudocolor plots of the current density components (Figs. 3 and 4) confirmed the effect of the degraded edges, it was found that the current density is quite more sensible to detect the roughness and the inhomogeneity.

The first part of the simulation consisted on the increment of the magnitude of the external field and, as expected, the distribution of magnetic induction was homogenized. As the external field was decreased there was a transition field where the current changed of direction and the magnetic induction and current distributions became homogenized.

Finally, when the external field was turned off, the remanent field distribution maintained traces of roughness, causing the magnetization to be higher compared to the case of a homogeneous superconductor. This last fact suggests to carry out studies considering an entirely inhomogeneous material (such as the YBCO monoliths), since in principle, higher magnetizations could be achieved if the inhomogeneity increases, thus improving its performance as superconducting magnets.

Acknowledgements

P. L. V. N. thanks CONACYT for the postdoctoral scholarship, as well as UABJO for the facilities granted. C. E. A. C. appreciates the hospitality and support provided by the UABJO.

1. S. Bhattacharya and M. J. Higgins, *Phys. Rev. Lett.* **70** (1993) 2617. https://doi.org/10.1103/PhysRevLett.70.2617
2. W. Henderson, E. Y. Andrei, M. J. Higgins and S. Bhattacharya *Phys. Rev. Lett.* **77** (1996) 2077. https://doi.org/10.1103/PhysRevLett.77.2077
3. A. Gurevich and V. M. Vinokur, *Phys. Rev. Lett.* **83** (1999) 3037. https://doi.org/10.1103/PhysRevLett.83.3037
4. M. A. Rongchao, *International Journal of Modern Physics B,* **28** (2014) 1450030. https://doi.org/10.1142/S0217979214500301
5. A. Lara, F. Aliev, A. V. Silhanek, and V. V. Moshchalkov *Sci. Rep.* **5** (2015) 9187. https://doi.org/10.1038/srep09187
6. A. H. Majedi, *Phys. Rev. Lett.* **127** (2021) 087001. https://doi.org/10.1103/PhysRevLett.127.087001
7. F. Wells, A. Pan, I. Golovchanskiy, S. A. Fedoseev, and A. Rozenfeld, *Sci. Rep.* **7** (2017) 40235. https://doi.org/10.1038/srep40235
8. J. R. Hull *Reports on Progress in Physics* **66** (2003) 1865-1886 https://doi.org/10.1088/0034-4885/66/11/R01
9. J. H. Durrell *et al*., *Supercond. Sci. Tech.* **31** (2018) 103501. https://doi.org/10.1088/1361-6668/aad7ce
10. M. Eisterer, S. Haindl, T. Wojcik and H. W. Weber *Supercond. Sci. Tech.* **16** (2003) 1282-1285. https://doi.org/10.1088/0953-2048/16/11/005
11. K. Zmorayova, L. Vojtkova, T. Hlasek, J. Plechacek and P. Diko *Supercond. Sci. Tech.* **33** (2020) 034005 https://doi.org/10.1088/1361-6668/ab6243
12. M. Lojka, T. Hlásek, F. Antoncík, A. M. Lauermannova and O. Jankosky *AIP Conference Proceedings* **2305** (2020) 020010 https://doi.org/10.1063/5.0033872
13. V. Antal *et al*., *Supercond. Sci. Technol.* **33** (2020) 044004 https://doi.org/10.1088/1361-6668/ab714f
14. C. Romero-Salazar *et al*., *Acta Physica Polonica A* **130** (2016) 645-648. http://dx.doi.org/10.12693/APhysPolA.130.645
15. C. Romero-Salazar, O. A. Hernández-Flores, O. Chumak, F. Pérez-Rodríguez and V. Chabanenko *J. Appl. Phys.* **122** (2017) 143904. https://doi.org/10.1063/1.4994905
16. T. Hirano, H. Fujishiro, T. Naito and M. D. Ainslie *Supercond. Sci. Tech.* **33** (2020) 044003. https://doi.org/10.1088/1361-6668/ab7297
17. E. H. Brandt, *Phys. Rev. B* **59** (1999) 3369-3372. https://link.aps.org/doi/10.1103/PhysRevB.59.3369
18. P.H. Kes, J. Aarts, J. van den Berg, C.J. van der Beek, and J.A. Mydosh, *Supercond. Sci. Technol.* **1** (1989) 242-248. https://doi.org/10.1088/0953-2048/1/5/005
19. O.I. Lyubimov, I.O. Lyubimova, V.A. Yampol'skii, and F. Pérez-Rodríguez, *Rev. Mex. Fís.* **43** (1997) 592-597. https://rmf.smf.mx/ojs/index.php/rmf/article/view/2688/2656
20. M. Smith, A. V. Andreev, M. V. Feigel'man, and B. Z. Spivak, *Phys. Rev. B* **102** (2020) 180507(R). https://doi.org/10.1103/PhysRevB.102.180507

21. W.E. Schiesser, and G.W. Griffiths, A Compendium of Partial Differential Equation Models: Method of Lines Analysis with Matlab (New York: Cambridge University Press, 2009), pp. 1-17.